Title

Modeling CO2 Hydrogenation to Methanol on an Ensemble of Inverse ZrO2 on Cu Catalytic Sites: Mechanism, Reactivity, and Deactivation

Journal

Angewandte Chemie

ISSN

0044-8249

Authors

Yang, Zihan
Alexandrova, Anastassia N
Sautet, Philippe

Publication Date

2026-06-03

DOI

10.1002/ange.5448247

Title: Modeling CO_2 Hydrogenation to Methanol on an Ensemble of Inverse ZrO_2 on Cu Catalytic Sites: Mechanism, Reactivity and Deactivation

Zihan Yang[a], Anastassia N. Alexandrova[a,b,c]*, Philippe Sautet[a,c,d]*

[a] Department of Chemistry and Biochemistry, University of California, Los Angeles, CA 90095, United States

[b] Department of Materials Science and Engineering, University of California, Los Angeles, CA 90095, United States

[c] California NanoSystems Institute, University of California, Los Angeles, CA 90094, United States

[d] Department of Chemical and Biomolecular Engineering, University of California, Los Angeles, CA 90095, United States

*Corresponding Authors: ana@chem.ucla.edu, sautet@ucla.edu

Abstract: Inverse ZrO_2/Cu catalysts, where Zr oxide is deposited on Cu particles, show a high catalytic performance converting CO_2 to methanol. We employ density functional theory (DFT) calculations to investigate the CO_2 hydrogenation reaction mechanisms on a model of highly dispersed Zr oxide clusters on Cu (111). The exploration is not performed on a single active site configuration but across an ensemble of 83 formate configurations accessible under reaction conditions. Detailed reaction-pathway analysis reveals that structural sensitivity is pronounced, and only 10 of the catalyst configurations are significantly active across the full pathway. The turnover frequency of the studied inverse structures is largely determined by reaction steps after methoxy formation, rather than the formate hydrogenation steps, and the energy of the methoxy intermediate is a key reactivity descriptor. Two hypotheses are presented for the ensemble average activity: where the probabilities of site populations are determined at the formate intermediate, or at the methoxy resting state. The latter, compared to the former, drastically changes the site distribution, eliminating active structures and decreasing the average rate by a factor 1000. Catalyst rigidity helps maintain activity by slowing down the structural evolution from the more active formate-bound states to the less active methoxy-bound states.

I. Introduction:

The rapid increase in anthropogenic CO_2 emissions from fossil fuel use has intensified concerns over global warming.[1, 2] Converting CO_2 into value-added chemicals offers a viable route to valorize CO_2 waste, mitigate emissions and contribute to a closed carbon cycle.[3-6] Methanol is a particularly attractive product for near-term commercialization due to its role as a versatile chemical feedstock and clean energy carrier.[7-10] Hydrogenation of CO_2 is challenging due to its high thermodynamic stability and the presence of additional kinetic barriers in the reaction pathway, making development of high performance catalyst a major research target.[7, 11] The industrial catalyst is formed by Cu nanoparticles on oxide supports (Cu/oxide).[12] Formate is a key intermediate in the CO_2 hydrogenation pathway, but on most Cu/oxide catalysts it is often over-stabilized, requiring elevated temperatures for further conversion.[13-15] Specifically, copper–zirconia catalysts are widely recognized for CO_2 hydrogenation to methanol, valued for their high stability in the steam-rich environments produced under reaction conditions.[14, 15] On conventional Cu/ZrO_2 catalysts (Cu supported on ZrO_2), the activated *CO_2 is hydrogenated to formate and then methoxy at the interfacial sites.[16, 17] Most literatures reported that hydrogenation of formate is the rate determining step on the conventional Cu/ZrO_2 catalysts, [16-18] and optimization of the interface structure is the key to enhance the conversion rate of surface oxygenate intermediates.[19] For efficient methanol synthesis under low-temperature conditions, it is therefore desirable either to bypass the conventional formate route via an alternative reaction pathway or to modify the adsorption configuration of formate to lower its conversion barrier.[20-22] To this end, efforts have focused on developing novel catalytic materials through strategies such as tailoring the metal composition, optimizing preparation methods, and introducing suitable promoters.[23-25]

Recently, an inverse catalyst structure, featuring an oxide on metal configuration, was proposed, offering an enhanced control over the interfacial sites.[26-28] Wu et al. reported that a ZrO_2/Cu inverse catalyst with highly

dispersed Zr species (~10% surface coverage) on Cu achieved a three-fold increase in methanol yield compared to the conventional Cu/ZrO_2 catalyst.[29] Similarly, Xu et al. showed that tuning the precipitation sequence and ratio of Cu and Zr precursors transformed the conventional Cu/ZrO_2 interface into a Cu-supported nano-ZrO_2 inverse interface, which strengthened the ZrO_2–Cu interaction and likewise boosted methanol productivity by more than three-fold.[19] Together, these studies demonstrate that the inverse ZrO_2/Cu configuration consistently enhances interfacial synergy and markedly improves methanol synthesis performance.

While existing literature agrees that interfacial sites on Cu and ZrO_2 catalyst are important for catalytic activity, the reaction mechanism for inverse catalysts remains a matter of debate. For conventional Cu/ZrO_2 catalysts, both *in situ* DRIFTS measurements and computational studies have consistently identified formate hydrogenation as the rate-determining step.[11, 18, 19, 30] However, evidence for the inverse catalysts ZrO_2/Cu is less consistent. Kattel et al., based on *in situ* DRIFTS data and DFT simulations, concluded that the high stability of the formate intermediate hinders its conversion and limits catalyst activity.[30] In contrast, Wu et al. and Xu et al. reported that formate species in the inverse configuration are reactive, with the conversion from formate to methoxy being kinetically easier than the subsequent methoxy-to-methanol step.[11, 19, 29] These contrasting observations suggest that changes in catalyst configuration may lead to a fundamental shift in the reaction mechanism. Given these discrepancies, a detailed computational study on the reaction mechanism using catalyst structures present under realistic conditions is needed. Unlike experimental IR studies, which average on configurations and can only indirectly infer intermediate structures and energetics, computational modeling allows each catalyst configuration and elementary step to be simulated explicitly and the associated structures along the reaction pathway to be visualized directly. Such an approach, although challenging if a large number of catalyst configurations and a complex mechanism are involved, can provide the mechanistic clarity needed to resolve the current ambiguities surrounding the inverse ZrO_2/Cu catalyst system.

In previous work, we showed that highly-dispersed ZrO_2/Cu presents a large ensemble of configurations involving formate intermediates and investigated a single elementary step, the mono-hydrogenation of formate, on this ensemble of inverse ZrO_2/Cu catalyst configurations under reaction conditions of P = 4.93 atm, conversion = 0.8%, CO_2/H_2 ratio = 1:3, and T = 493.15 K.[31-33] The ensemble was generated by DFT-based basin-hoping simulations at these conditions for Zr_3 clusters on Cu(111) with variable numbers of O, OH and formate ligands. We observed that the activity for the formate hydrogenation elementary steps strongly varies across the ensemble and even among sites within the same catalyst configuration, with formates that can hydrogenate fast (barriers of ca 0.8 eV) and formates that would react very slowly (barriers of more than 1.3 eV). Notably, metastable structures were found to dominate the overall ensemble activity for formate elementary hydrogenation step.[31] In the present study, we build upon those findings by performing a detailed exploration of the entire CO_2-to-methanol reaction mechanism on all these catalysts configurations. The overall CO_2 hydrogenation mechanism was considered in two stages: (i) hydrogenation of formate to form the methoxy intermediate, and (ii) hydrogenation of methoxy to yield methanol as the final product. As described before, while experiments on conventional Cu/ZrO_2 catalysts and some on inverse configurations suggest that formate hydrogenation is the rate-determining step, other studies on inverse catalysts indicate otherwise. Through a comprehensive computational analysis of the ensemble of catalyst structures, we address this mechanistic ambiguity for ZrO_2/Cu inverse catalysts. Our mechanistic analysis reveals that, under the selected reaction conditions, various structures in the catalyst ensemble present markedly different reactivity, with only a few metastable highly active inverse catalyst structures that all exhibit the TOF-determining transition state (TDTS) during the stage of hydrogenation of methoxy to methanol. The reactive structures feature partially reduced Zr clusters and reactive site located at a moderate distance to the Cu support, typically in the range of 3.5–4.0 Å. We show that the energy of the methoxy intermediate plays a key role for the reactivity and that slow conversion of catalyst structures from these with moderately stable methoxy to those with highly stable methoxy represent a microscopic mechanism for deactivation.

II. Computational methods. The DFT calculations were performed using the Vienna Ab Initio Simulation Package (VASP) with the projector augmented wave (PAW) formalism to describe electron–ion interactions.[34, 35] Exchange–correlation effects were treated using the Perdew–Burke–Ernzerhof (PBE) functional.[36] Dispersion corrections were included using the dDsC approach.[37] The plane-wave basis set was truncated at a kinetic energy cutoff of 400 eV. The Brillouin zone was sampled using a 3×3×1 Monkhorst–Pack grid for all slab models. A Gaussian smearing of 0.1 eV was applied to aid k-point convergence. A Hubbard *U* correction, U_{eff} = U − J, of 4.0 eV was applied to the Zr 4d orbitals.[38] . Dipole corrections were applied to limit spurious dipolar interactions between slabs. The convergence

criteria for the force and electronic energy convergence were set to 0.02 eV/Å and 10^{-6} eV, respectively. Transition states were located using the climbing image nudged elastic band (CI-NEB) method with eight intermediate images connecting the reactant and product states, and were validated through vibrational frequency analysis.[39]

The modeled catalysts feature a zirconium cluster composed of three Zr atoms, with varying coverages of formate (HCOO), hydroxyl, and oxygen species, supported on the Cu(111) surface. The Cu(111) support was represented using a 5×5 supercell, each repeat vector measuring 12.76 Å, and composed of five atomic layers. During structural optimization, the bottom two copper layers were kept fixed while the remaining layers were allowed to relax. A vacuum space of 20 Å was included along the z-axis in all models to prevent undesired interactions.

The reaction conditions are characterized by four key parameters: (a) total pressure, (b) the CO_2:H_2 ratio in the initial feed, (c) the temperature at which the reaction is conducted, and (d) the conversion of the reaction shown in the following equation, which provides the partial pressures of reactants and products:

$CO_2 + 3H_2 \rightarrow HCOO + 2.5H_2 \rightarrow CH_3OH + H_2O$

The chemical potential of O, μ(O) is calculated using the formula $\mu(O) = \mu(H_2O) - \mu(H_2)$. The chemical potential of OH is calculated using the formula $\mu(OH) = \mu(H_2O) - 0.5\mu(H_2)$, and the chemical potential of HCOO is calculated using the formula $\mu(HCOO) = \mu(CO_2) + 0.5\mu(H_2)$. Thermodynamic calculations are conducted to determine chemical potentials of H_2, H_2O, CO_2, and CH_3OH. They are treated as ideal gases at experimental temperature and pressure, and translational and rotational entropy are considered.

III. RESULTS AND DISCUSSION

III.1 REACTION PATHWAY EXPLORATION

In the considered reaction conditions (P = 4.93 atm, conv = 0.8%, CO_2/H_2 ratio = 1:3, and T = 493.15 K), from our previous extensive grand-canonical basin hoping exploration, the $Zr_3O_x(OH)_y(HCOO)_z$ model on Cu(111), with varying x, y, and z values and different geometries, presents a large ensemble of free energy accessible configurations.[32] Altogether 83 catalyst configurations, each binding 2 to 4 formate moieties, are found in an energy range of only 0.2 eV from the global minimum. We use this ensemble to determine catalyst configurations active for the CO_2 hydrogenation to methanol. Each configuration will be labelled by its rank according to the free energy of this formate state. Due to the formidable task of exploring this multistep reaction on a large number of configurations, we conducted a hybrid approach determining the complete pathway on a set of active configurations, while all others being rigorously eliminated because at least one step had a too high barrier to efficiently contribute to the overall reaction rate. From our previous investigation of the formate mono-hydrogenation elementary step, 14 reactive catalyst configurations with a relative contribution to the average rate constant of that step exceeding 0.02% were initially selected.[31, 32] These formate structures are all accessible in reaction conditions, especially when considering typical error bars in the PBE DFT method used. Other configurations can be safely excluded since their barrier for the formate hydrogenation elementary step is too high to provide a good overall rate for the CO_2 hydrogenation reaction. Reaction-pathway analysis has been performed on this set of 14 reactive structures, with an objective to identify the most favorable reaction pathways across these configurations and assess whether a consistent reaction sequence emerges among the most active structures.

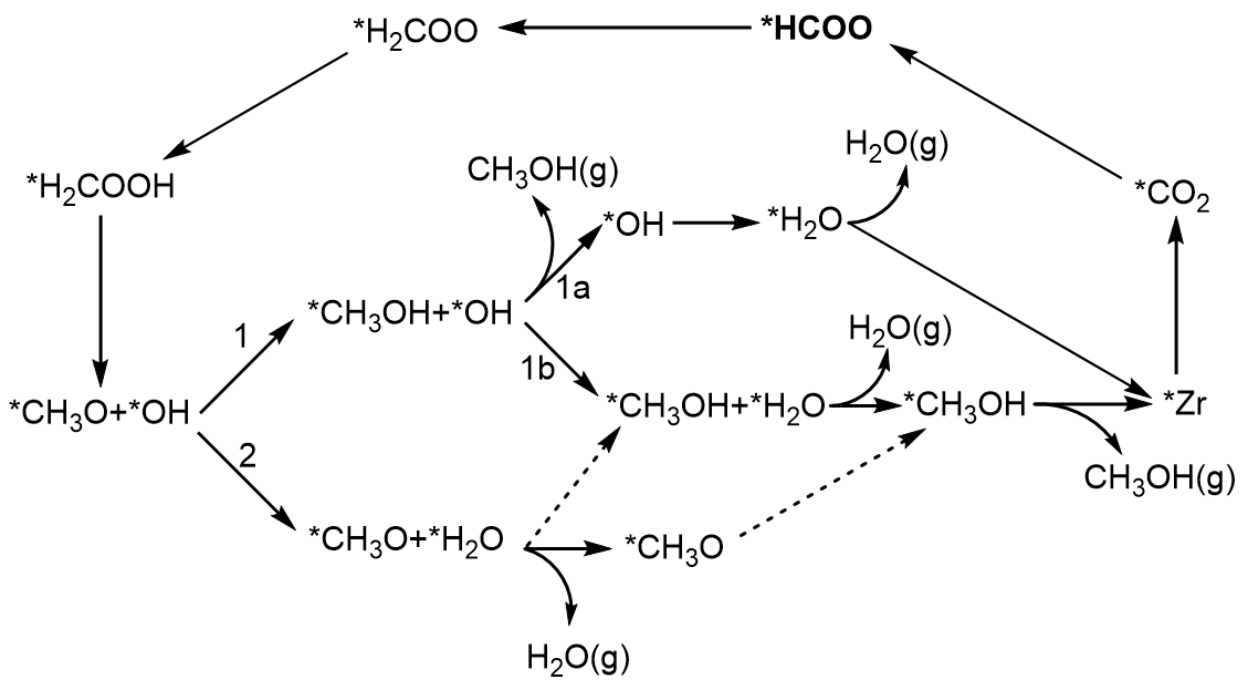

Scheme 1: The main reaction pathways for the explored formate mechanism of CO_2 hydrogenation to methanol. * Indicates an absorbed species and *Zr represents the unsaturated catalyst configuration after methanol desorption. Hydrogen adsorption is not explicitly indicated.

The reaction network for the formate mechanism of CO_2 hydrogenation to methanol is recalled in scheme 1. The explored catalyst configurations contain two to four formate species. For each structure, we enter the catalytic cycle with the most reactive formate, which is hydrogenated preferentially to H_2COO (from our previous work).[31] This hydrogenation step occurs at the interface between the $Zr_3O_x(OH)_y(HCOO)_z$ cluster and the Cu surface, with the formate being bound to the Zr_3 cluster, while the H atom (initially formed by H_2 dissociation) being on the Cu surface and diffusing towards the interface. All further hydrogenation steps in the mechanism occur similarly. The H_2COO intermediate is then further hydrogenated to H_2COOH. After this point, two mechanistic possibilities are examined: (i) cleavage of the O–O bond in H_2COOH to generate $*H_2CO$ and *OH, or (ii) a concerted hydrogenation and bond-cleavage step forming $*CH_3O$ and *OH. All structures consistently showed preference for the 2nd possibility with lower energy barriers. After formation of the methoxy intermediates, the reaction can proceed toward either methanol (pathway 1 in Scheme 1) or water formation (pathway 2 in Scheme 1). Along pathway 1, the sequence diverges into two sub-routes: in pathway 1a, methanol desorbs first followed by water formation; in pathway 1b, water forms while methanol remains adsorbed, after which methanol and water desorb sequentially. In pathway 2, water forms first; water desorption leaves behind a stabilized methoxy species which is afterward hydrogenated to methanol, which then desorbs. At this point the pathways reconverge, the now vacant *Zr site subsequently binds and activates CO_2, regenerating the formate species, marking the complete cycle for the most reactive formate. The full set of reaction pathways on the 10 most reactive catalyst configurations (1, 3, 5, 6, 13, 22, 25, 34, 59, 61, see table 1), including all intermediates and transition states, is provided in Figures S1–S10 and the explored stage of the 4 eliminated structures, due to too high barriers, are shown in Figure S11. Two representative examples for pathways 1a, 1b, and 2 are shown in Figure 1. Figure 1a illustrates the pathways initiated at the most reactive formate of the catalyst structure 5, 0.035 eV above the global minimum for the formate state, where the blue lines correspond to pathway 1a and the black lines to pathway 2 (pathway 1b shows a higher overall barrier than 1a and is discarded). The catalytic turn over frequency (TOF) will be evaluated here from the energetic span model[33] which estimates the catalytic turnover frequency (TOF) from the free-energy profile by identifying the turnover-determining transition state (TDTS) and intermediate (TDI), whose energy difference defines the energetic span (ΔG_{span}). The

TOF for one catalyst configuration i is calculated by using transition state theory $\mathrm{TOF_i} = \frac{\mathrm{kT}}{\mathrm{h}} \exp\left(-\frac{\Delta \mathrm{G_{span}}}{\mathrm{kT}}\right)$. The TDTS and TDI are indicated by stars on each energy reaction diagram.[33] For that purpose, we recall here, that in the case of a pathway that separates in two branches, the TDI corresponds to the lowest energy one of each branch, even if the TDTS is on the other branch. Structure 5 is representative of structures that feature an overly stable methoxy intermediate in pathway 2, which leads to a high energetic span and a slow turnover frequency. Figure 1b presents the pathways for the most reactive formate on the catalyst structure 34 (energy 0.114 eV above the global minimum), with pathway 1b plotted in orange and pathway 2 in black. Structure 34 serves as an example of structures that have a less stable methoxy intermediate, and thus a smaller energetic span and faster turnover frequency.

Table 1 Ligand numbers for the formate structure, formate state relative free energy and methoxy state relative free energy for the 10 most reactive catalyst structures. All structures contain 3 Zr and are supported on Cu(111). Free energies are evaluated using the considered reaction conditions (P = 4.93 atm, conv = 0.8%, CO_2/H_2 ratio = 1:3, and T = 493.15 K), details included in SI Note 1.

Formate structure free energy ranking	Formate structure formula	Formate state relative free energy (eV)	Methoxy state relative free energy (eV)
1	$O_3(OH)_2(HCOO)_4$	0	0.34
3	$O_3(OH)_2(HCOO)_4$	0.023	0.52
5	$O_3(OH)_2(HCOO)_4$	0.039	0
6	$O_3(OH)_3(HCOO)_3$	0.055	0.775
13	$O_2(OH)_4(HCOO)_3$	0.079	0.34
22	$O_3(OH)_3(HCOO)_3$	0.079	0.36
25	$O_3(OH)_2(HCOO)_4$	0.092	0.02
34	$O_3(OH)_3(HCOO)_3$	0.114	0.77
59	$O_1(OH)_5(HCOO)_3$	0.188	0.45
61	$O_2(OH)_3(HCOO)_4$	0.193	0.246

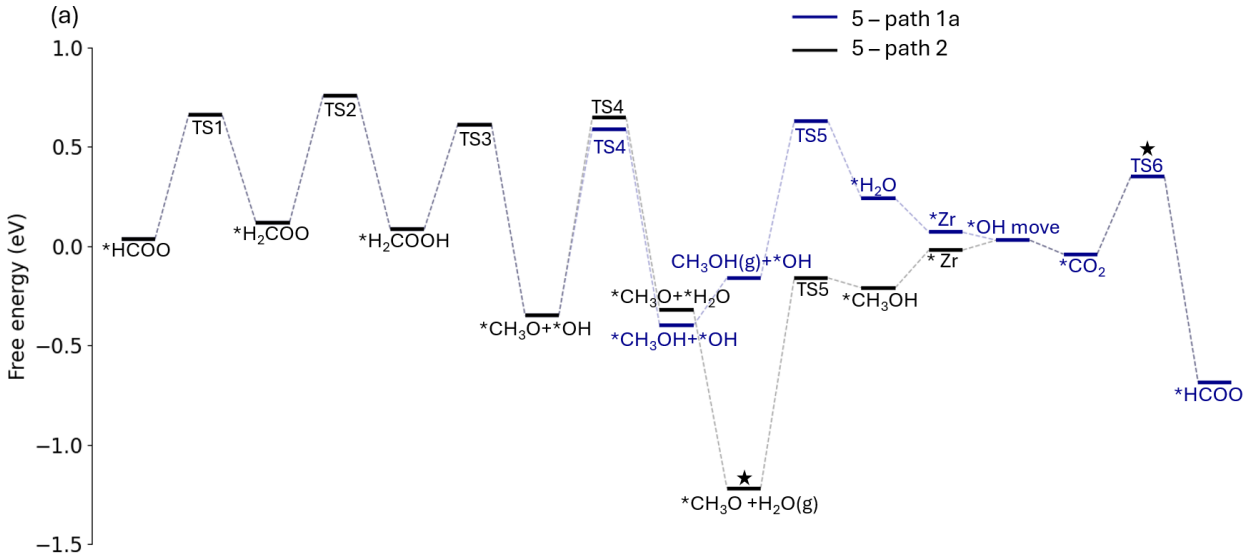

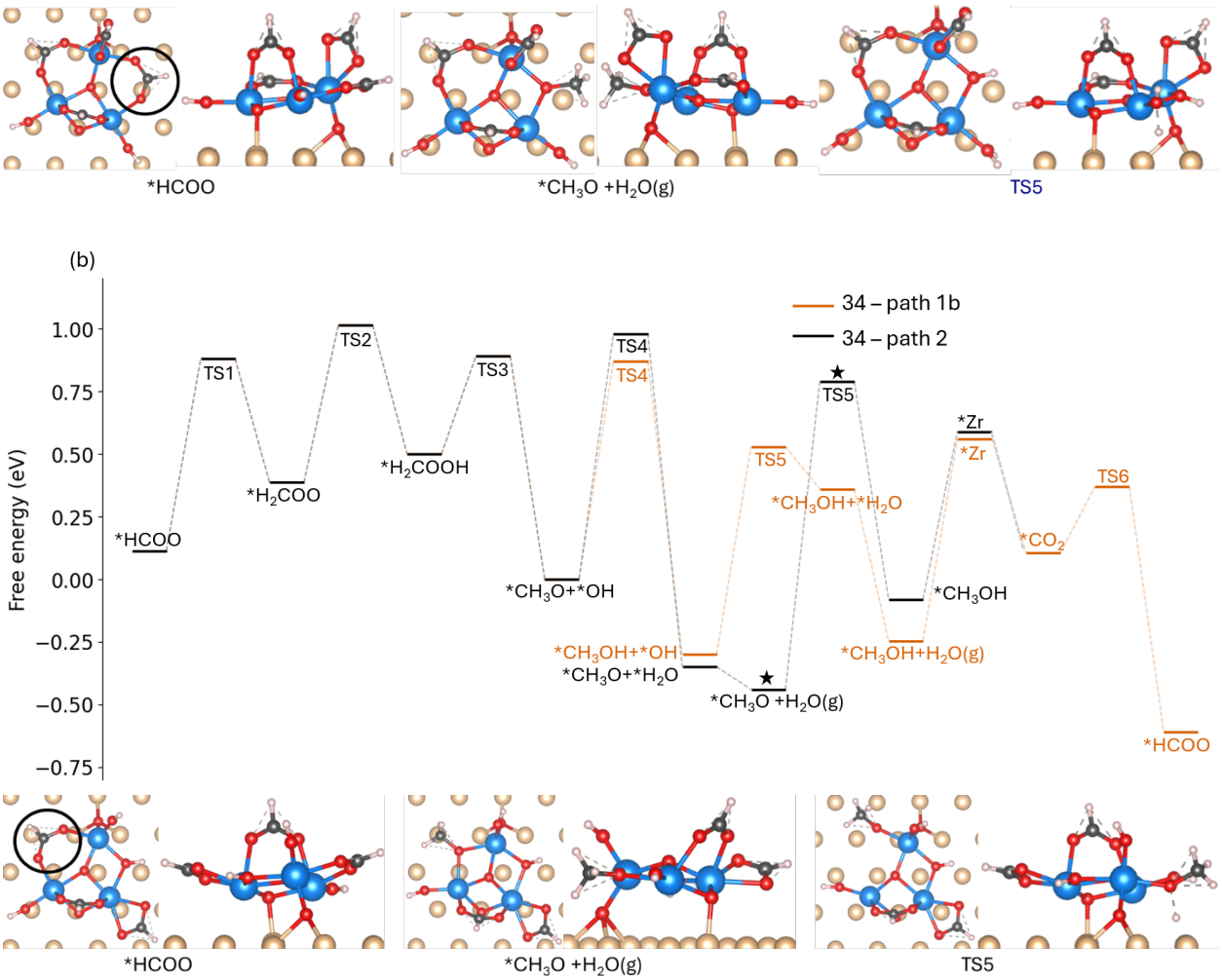

Figure 1. Reaction pathway examples on two catalyst configurations representing pathway 1a, 1b, and 2 in Scheme 1 under reaction condition P = 4.93 atm, conv = 0.8%, CO_2/H_2 ratio = 1:3, and T = 493.15 K. (a) Reaction pathway initiated at the most reactive formate of catalyst structure 5, representing pathway 1a in blue and 2 in black. (b) Reaction pathway initiated at the most reactive formate of catalyst structure 34, representing pathway 1b in orange and 2 in black. The intermediate and transition state determining the apparent energetic span and therefore the TOF are labeled with stars, and the relevant structures are shown. The reactive formate is shown in a black ellipse in the structures on the left.

III.2 Catalytic Activity

The individual TOF values for each of the 10 active catalyst structures are shown in Figure 2a together with the corresponding apparent activation energies (energetic spans). For all 10 reactive catalyst configurations, the TOF-determining intermediate (TDI) is the stable methoxy intermediate in pathway 2, which lies in the second stage of the reaction, from methoxy to methanol formation (see Figure 1 for catalyst structures 5 and 34, and Figure S1-11 for all other structures). For most of the reactive structures, the TOF-determining transition state (TDTS) are in the second stage of reaction, as it is the case for catalysts 5 and 34 in Figure 1), and only the TDTS for catalyst configurations 1, 13 and 22 are placed in the first stage of formate hydrogenation (Figure S1, S5, S6).

The major rate contributors among the catalyst ensemble are metastable structures 6 and 34, with a free energy of the formate state of 0.039 eV and 0.114 eV above the global minimum 1, while this global minimum has a much

lower reactivity. The energy of the methoxy intermediate in pathway 2 is a key descriptor of the catalytic activity, and many structures (as #5 in Figure 1) are deactivated by the high stability (low free energy) of the methoxy intermediate in pathway 2, which increases the energetic span. On the other hand, for the most active catalyst structures (such as #34 in Figure 1), the methoxy intermediate shows a moderate stability and impacts less negatively on the reaction rate. Variations in the free energy of the methoxy intermediate as a function of catalyst configurations are large, up to 0.8 eV. Although configurations 5, 25 and 61 (with energy 0.035, 0.092 and 0.193 eV respectively) are highly reactive for the first reaction stage of formate hydrogenation to methoxy,[31] their strongly stabilized methoxy intermediates and therefore poor activity for the second stage (from methoxy to methanol) result in a low **overall** rate.[31] Besides methoxy, other species are present on the Zr_3 cluster for the TDI structure during reaction (O, OH, non-reactive formates) and these other ligands also contribute to the stability of the "methoxy" intermediate.

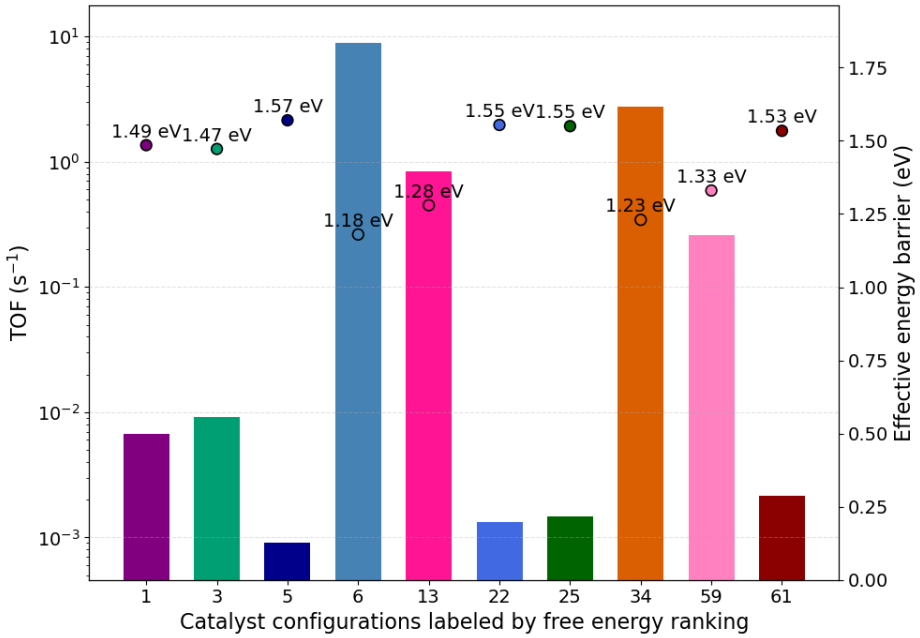

Figure 2. Individual catalytic activity of each reactive catalyst configuration. TOF (s^{-1}, in log scale) per zirconia cluster for each structure with their energy ranking in the formate state labeled on x-axis. The apparent activation energies are labeled above the TOF bars. The main contributors are catalyst structures 6 followed by 34.

For all catalyst structures with high TOF, the TDTS is in the second stage of reaction from methoxy to methanol. This indicates that the hydrogenation of formate is not the rate determining step, which is consistent with experimental studies on inverse ZrO_2/Cu catalysts.[11, 19, 29] In contrast, experimental comparisons between inverse and conventional configurations report that on conventional catalysts, the formate intermediate is highly stable, making its hydrogenation rate determining.[16, 18, 19] DFT studies by Yu et al. and Lamier et al. found that oxygenated intermediates are much more stable on conventional Cu/ZrO_2 catalysts compared with oxygenates on the inverse catalyst, making formate hydrogenation the RDS in the conventional Cu/ZrO_2 systems.[16, 18]

To understand the factors that influence the stability of the methoxy intermediate in pathway 2, we examined several parameters (Figure S12), including the Bader charge of the Zr atom connected to the methoxy group, the average Bader charge of the Zr cluster, the distance between the methoxy group and the Cu surface, and the Bader charge of the oxygen atom. A random forest regression analysis shows that the distance from the methoxy group to the Cu surface is the most important factor for the stability of the methoxy intermediate in pathway 2. The shorter the distance, the more stable the methoxy is, as shown in Figure S12b. Bader charge of Zr and O on the methoxy have less importance. The formate species on active sites with high activity for the overall reaction exhibit two key

structural features: (1) they adopt an orientation that is approximately parallel to the Cu surface, and (2) they maintain a moderate distance, close to the surface but not excessively short, typically in the range of 3.5–4.0 Å (between the O on methoxy and Cu surface). This balanced geometry facilitates efficient hydrogenation by allowing sufficient interaction with H on the Cu surface while preventing the high stability of the methoxy intermediate. This distance could be a target for inverse design of active interfaces, changing the size of the Zr cluster, the type of Cu surface or the experimental conditions. Electronically, active sites are characterized by a partially reduced Zr cluster adjacent to a metallic Cu surface, which together provide the optimal charge distribution to stabilize the reactive formate and promote subsequent hydrogenation steps.

Going from the TOF of individual catalyst configurations to the average ensemble TOF on the catalyst requires to assess the probabilities to find a given catalyst configuration during reaction. This is highly challenging since one needs to determine the nature of the resting state of the catalyst during reaction, and that this might depend on the catalyst configuration considered. The formation of formate is very fast from CO_2, as seen by the low barriers (0.3-0.6 eV, see Figures S1-10). For some catalyst configurations and some formates, the further hydrogenation to methoxy is associated with high barriers and very slow kinetics, so that the formate state would be the resting state. For other catalyst configurations or other formate species, as shown in this paper, methoxy will form at a reasonable rate and will be the TOF limiting intermediate, therefore the resting state. A realistic description of the catalyst during reaction would therefore contain a mixture of formate and methoxy resting states.

Another difficulty is that the catalyst configurations are not static but will evolve with time by conversion from one configuration to another. Note that catalysts structures might not have the same composition in terms of number and type of ligands, so that catalyst structure conversion is not necessarily an isomerization. It is known that the preferred cluster catalyst structure depends on the nature of the bound intermediate, i.e., in the thermodynamic limit (or equivalently, given infinite amount of time), there will be a reorganization of the catalyst towards more stable configurations associated to a novel resting state, such as methoxy on some of the isomers.[40, 41] The key question is to determine the time scale of catalyst restructuring, and compare it with reaction time scale (TOF of the order of $1s^{-1}$) or with the reactor time scale (many days). We will show with a few examples in the next section that conversion barriers for the ZrO_x/Cu catalysts are typically high, in the order of 1.8 eV which at reaction temperature corresponds to a reaction time of about 10 days. Hence, we can assume that the time scale for configurational transformation of catalyst is much longer than the CO_2 hydrogenation reaction time scale. In this case, each configuration reacts without conversion.

A final difficulty is that probability of presence shows an exponential dependence on free energy, in Boltzmann statistic. However, DFT has limited accuracy, and errors of even 0.1 eV would provide drastic changes in the calculated probabilities.

Therefore, we will adopt here a qualitative approach and compare two hypotheses. In the first approach, we will consider that probabilities are determined by a pre-equilibrium for the formate structures of our 83 catalyst configurations, by using Boltzmann statistics, and that these probabilities are then fixed during reaction. The second approach will start with these formate state distribution, and reweigh the 10 reactive configurations of Figure 2 to the probabilities arising from the stability of their methoxy state, instead of their formate state, keeping the probabilities of all other configurations to the value of the formate state equilibrium. This second approach models a mixture of low reactivity formate configurations and of methoxy states for the more active ones, as discussed above.

For all cases, since each configuration reacts without isomerization in the reaction time-scale, the average TOF can be calculated by $\mathrm{TOF_{av}} = \sum \mathrm{P_i} \times \mathrm{TOF_i}$, where i runs on all configurations, Pi is the probability of this configuration and TOF_i is its individual TOF (low reactivity configurations not shown in Figure 2 are assumed to have the TOF of zero). The total list of configurations, with their probabilities in the two approaches is provided in the SI. Probabilities are supposed to be normalized, i.e. their sum for the 83 catalyst configurations is equal to 1.

In Figure 3a, the shaded bars show the probability weighted TOF, $P_i \times TOF_i$ for the 10 active catalyst configurations in both approaches described above, while Figure 3b and c show the contribution of these active catalyst structures to the average TOF. If we first consider the probabilities determined by pre-equilibrium of formate structures, the overall rate is dominated by the contribution of catalyst structure 6 (90%), which is also the most active *individual* structure (Figure 2), while structures 13 and 34 contribute both for ca 5% (Figure 3b). The average TOF is 0.14 s^{-1} per Zr and its order of magnitude is close to that from experimental measurements for inverse ZrOx/Cu catalysts.[11, 19, 42] In contrast, changing to probabilities based on the methoxy intermediate free energy for the 10 reactive configurations strongly affects the simulated reactivity. The average TOF drops to 0.00014 s^{-1} per Zr. Previously highly reactive configurations (such as 6 or 34) show moderately stable methoxy TOF-determining intermediates, and their probability based on methoxy state energy becomes very small. The previous leading configuration 6 for example sees its probability dropping by a factor of ca. 10^{-7}, and its contribution to the rate becomes negligible (Figure 3c). The configurations with highly stable methoxy intermediates (such as 5 and 25) dominate the probability and the contribution to the average TOF, but their intrinsic individual activity is low, of the order of 10^{-3} s^{-1}.

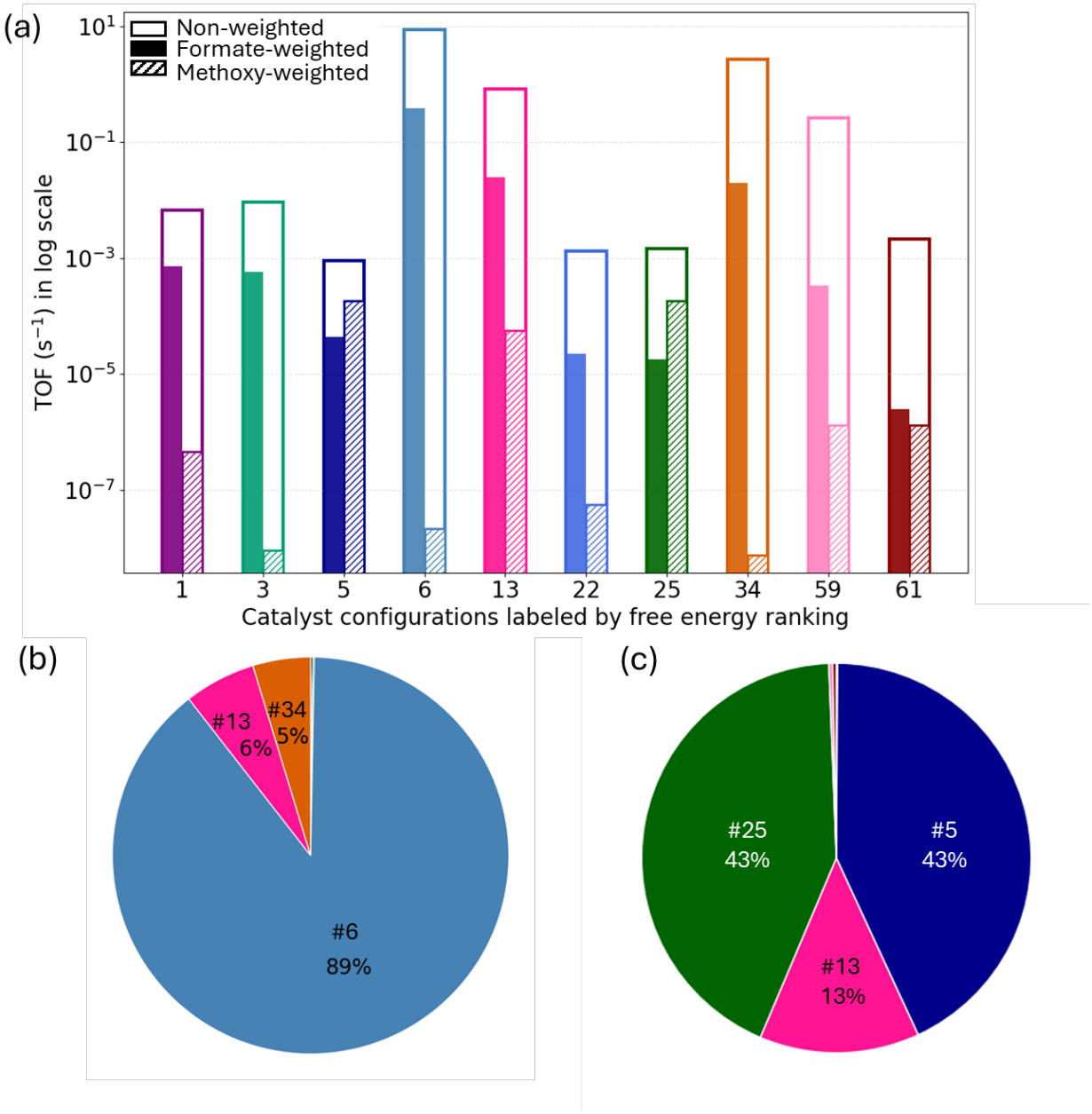

Figure 3. Probability weighted TOF and distribution. (a) Log scale of TOF_i for each structure weighed by the formate structure probability with their free energy ranking on the x-axis. Bars with colored borders and no fill recall unweighted TOF while the solid-colored bars are formate probability-weighted TOF, and the shade bars are methoxy probability-weighted TOF. (b) Contribution of catalyst configurations to the overall rate using probabilities based on the formate state free energy. The main contributors are in decreasing order catalyst structures 6, 34 and 13. (c) Contribution of catalyst configurations to the overall rate using probabilities based on the methoxy state free energy. The main contributors are in decreasing order catalyst structures 25, 5 and 13.

Therefore, equilibrating the reactive configurations in the methoxy resting state drastically changes their distribution, eliminating active structures with moderately stable methoxy. However, the catalyst structure isomerization required to reach the methoxy-based probability is slow, so that the catalyst structure will initially operate out of equilibrium, with the distribution of sites prescribed at the formate-bound state. This provides a hypothesis for the microscopic view of one catalyst deactivation mechanism. The catalyst can initially be described

by an ensemble of configurations, some of them presenting high activity and moderately stable TOF determining intermediate (methoxy in our case). Configurations with more stable TOF determining intermediate and low activity are thermodynamically favored, and their population will slowly increase at the expense of the active ones, leading to a slow deactivation of the catalyst. A certain rigidity in the catalyst and strong binding of the spectator adsorbates therefore appears beneficial, to provide sizeable isomerization and ligation change barriers, leading to slow isomerization and deactivation. Very fluxional catalysts would in contrast tend to equilibrate fast, and quickly transform into configurations with stable resting states, but low activity.

III.3 Exploration of conversion pathways

To justify our hypothesis about the slow conversion of the catalyst, pinning the catalyst to a given configuration during the catalytic cycle, we examined the possibility of conversion between catalyst configurations at a given point of the reaction, i.e. at given reaction intermediates. To assess this, we carried out simulations on selected initial configurations and reaction intermediates where isomerization could be possible. Configurations can present different numbers of O, OH and formate ligands, so that they are not mere structural isomers, and conversion is not straightforward. Ligand addition or removal requires several elementary steps, for example O removal goes through H_2O formation, by sequential H transfer coupled with electron transfer, and water desorption. Generally speaking, isomerization involves a set of elementary processes such as ligand addition reaction, ligand removal reaction and ligand displacement from one site to another. One difficulty is linked to the fact that a large number of ligands are placed on the Zr_3 center (between 8 and 10, depending on the structure). Therefore, displacing a ligand generally requires displacing another one at the same time. For example, isomerization might require swapping a formate and an OH ligands. We have selected two conversion processes to provide characteristic cases of required elementary reaction steps; the first one start with structure 6 and goes to structure 34, which presents the same stoichiometry, so that the transformation is an isomerization, without addition or removal of ligands. The second considers structure 3 (0.023 eV) and its transformation into 34, which requires the removal of one formate and the addition of one OH and isomerization. The isomerization pathway starting from structure 6 is shown in Figure 4. The isomerization requires switching position for a hydroxyl group connected at the lower right Zr with the vertical bidentate chelate(κ^2-O,O') formate connected to the top Zr from the top view. Direct through space switching between the two ligand is not possible. Two potential pathways for the isomerization were tested. One pathway involves a third ligand, which is a bridging OH between the two considered Zr centers. First, the vertical formate moves to the bridging position (μ-η^1: η^1) while the bridging hydroxyl group moves to the top Zr atom, through an exchange between the two ligands. Next, a second similar exchange occurs between the formed bridging formate and the OH group on the bottom right Zr. This process is significantly more difficult than hydrogenation, with isomerization effective barriers near 1.8 eV, compared to 1.57 eV for highest energy barrier of the hydrogenation reaction in Figure 2. Isomerization would therefore be ca 10^4 times slower than reaction. The other possible pathway first adsorbs a water on the top Zr atom, and then the hydrogen on water is transferred to the bridging OH, forming a bridging water, which is then desorbed. Then, the vertical formate moves to the bridging position. The following step would be swapping the newly formed bridging formate with the bottom OH. The initial steps of this pathway have higher energy barrier (1.91 eV) than the pathway shown in Figure 4 and the reaction profile is shown in Figure S13. For the transformation between 3 and 34, we first start at the resting state of the hydrogenation path, 3-*CH_3O, then hydrogenate it to *CH_3OH along the path and desorb methanol to obtain the unsaturated 3-*Zr intermediate. From there we do not absorb CO_2 to reform the formate, but form 34 by isomerization and OH addition (Figure S14). The first step is to shift a formate from a bidentate position on one Zr to a bridging configuration between 2 Zr. Due to the unsaturated nature of 3-*Zr, there is no ligand in the targeted bridge site, and the rearrangement is easy, with a barrier of 0.5 eV from 3-*Zr. The overall barrier from the methoxy resting state is 1.55 eV. The second step corresponds to binding water and then transferring an H atom to the Cu surface to form the OH ligand. The TS is 0.25 eV higher than the previous one, corresponding to an overall barrier of again 1.8 eV for the conversion. Therefore, the elementary transformations for conversion of one catalyst configuration to another involving rearrangements of adsorbates are shown on two examples to correspond to large barriers, and therefore should be kinetically slow compared to the hydrogenation reaction itself, supporting our hypothesis. The complete sampling

of all conversion pathways would make the picture more complete, but it is highly challenging and beyond the scope of this paper.

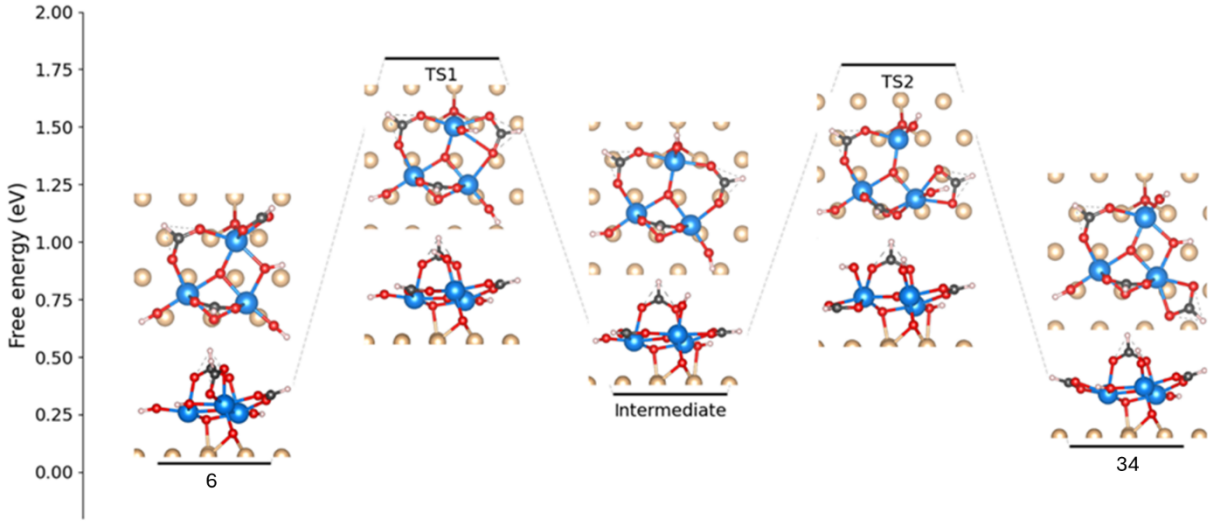

Figure 4. Slow structural transformation from structure 6 to 34, the energy barriers being much higher than that of the hydrogenation reaction.

III.4 Spectroscopic simulation of the state of the surface during reaction.

In this section we provide a link with experimental characterization by simulating the vibrational spectrum of the catalytic system in reaction condition. As explained earlier, the ZrOx/Cu inverse catalyst is formed by an ensemble of configurations with very diverse reactivity. Formate is formed quickly by CO_2 hydrogenation, but some formates/configurations will react further very slowly, for example the formate located far from the Cu support. In contrast the most reactive formate species react to form the stable methoxy, which further reacts less quickly. Our test calculations showed that forming two methoxy species on the same Zr trimer catalyst is not favorable, so this will not be included. IR simulations were performed for the stable methoxy intermediates for the 14 selected reactive structures and for the formate intermediates in the unreactive structures, since experimental IR primarily captures long lived species present at the time of measurement. Figure 5 presents the simulated IR spectrum during reaction, constructed using a Lorentzian broadening of 6 cm^{-1} and summing the contributions from structures accounting for 60% of the catalyst ensemble weighted by their Boltzmann probabilities for the formate intermediate, used as a model for the reactive state of the catalyst, i.e. before deactivation. In this IR spectrum, the peak around 1350 cm^{-1} associated with reactive formate vibrations per our previous paper[31] is gone, since the most reactive formates have been transformed into methoxy. The peaks from unreactive formate vibrations around 1360 cm^{-1} and 1530 cm^{-1} remain. Peaks from methoxy vibrations emerge at 1150 cm^{-1}. In experiments, in situ Diffuse Reflectance Infrared Fourier Transform Spectroscopy (DRIFTS) spectra showed methoxy peaks at 1147 cm^{-1} and 1154 cm^{-1}.[19, 29] The simulated IR agrees very well with the experimental DRIFTS, capturing the methoxy peaks and showing the disappearance of the most reactive formate species.[29] The in-situ DRIFTS after switching CO_2 inlet to He also showed the rapid consumption of the reactive formate, and slow consumption of the methoxy, indicating that the overall rate is governed by reacting the methoxy to the final product,[29] also in agreement with our mechanistic finding.

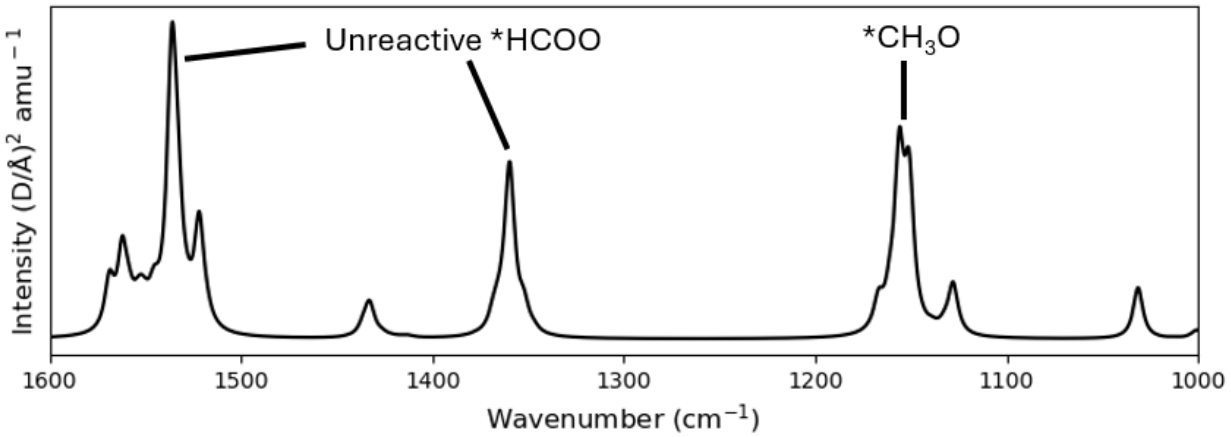

Figure 5. The simulated IR spectrum from the ensemble of catalytic species. Reactive formates are transformed into the TOF limiting intermediate methoxy (*CH_3O peak), while other non-reactive formates on the same structures and catalyst structures with inactive formate contribute to the symmetric (1340–1370 cm^{-1}) and asymmetric (1520-1580 cm^{-1}) stretching modes of formate.

IV. Conclusions

The catalytic reactivity of a large ensemble of model configurations for the inverse ZrO_2/Cu catalyst has been explored from DFT reaction pathway calculations. For this purpose, we used the ensemble of configurations determined previously for the formate state of the catalyst, with the model $Zr_3O_x(OH)_y(HCOO)_z$ on Cu(111), where the composition (x,y,z values) and geometry had been sampled by basin-hoping simulations.[32] This approach is validated a posteriori by the fact that CO_2 hydrogenation to formate is very fast so that the formate state is a good starting point. This ensemble is large with 83 catalysts structures, and our hybrid approach combined detailed reaction pathway simulations with early elimination of structures presenting at least one high barrier along the path. Rate evaluation with the energetic span approach shows that the ensemble of catalyst configuration presents a highly contrasted activity for CO_2 hydrogenation to methanol and that among the initial ensemble of 83 configurations, only 10 structures show a low enough energetic span (in the range 1.1-1-6 eV) to be significantly reactive. All these active configurations present the same TOF limiting intermediate, the methoxy intermediate in between formate and methanol on the path. The most active catalyst structures show the TOF-determining transition state in the second part of the pathway, between methoxy and methanol. This mechanistic picture is consistent with several experimental studies on inverse ZrO_2/Cu catalysts, which similarly identify post-methoxy transformations as the key steps controlling overall activity.[11, 19, 29] The energy of the TOF limiting methoxy intermediate is a key descriptor of the catalytic activity, and highly active configurations (6, 34) show moderately stable methoxy intermediates, while many catalyst structures (as 5, 25, 61) are deactivated by the high stability of their methoxy intermediate. Active formates lie flat, parallel to the Cu surface, but not too close to the Cu surface which favors a stable methoxy intermediate and decreases the activity for methanol. Activity of a catalyst structure is also favored by partially reduced Zr clusters.

Two approaches are considered to perform the ensemble averaging of catalytic activity. In the first one, configuration probabilities are calculated from the formate state of each catalyst configuration. The main contributions to the rate among catalyst structures are from configuration 6 (dominating) and from form 13 and 34 (smaller). The average rate is similar to the measured one and this distribution of catalytic sites can be considered as a model of the active state of the catalyst. However, active formate configurations will quickly convert to their methoxy intermediate and will not persist. In a second approach we therefore re-evaluate the probabilities of the 10 reactive configurations by considering the free energy of their methoxy state, i.e. assuming inter-conversion of the catalysts structures to reach the equilibrium for the methoxy state. This favors structures with stable methoxy intermediate and low hydrogenation activity, therefore completely changing the dominant contribution to the rate, to structures that had

a negligible role in the formate equilibrium state. The corresponding calculated rate for this ensemble decreases by a factor of ca 1000. From these findings, we conclude that the catalyst initially operates as an ensemble of configurations, some of which exhibit high activity with moderately stable methoxy intermediates determining the TOF. Over time, thermodynamically favored configurations with more stable methoxy resting states and lower activity become increasingly populated from inter-conversion between catalytic structures, leading to gradual catalyst deactivation. Structural rigidity and strong directional bonds to ligands are therefore beneficial, as they slow down catalyst isomer interconversion and delay the shift toward less active configurations.

Inter-conversion between catalytic structures requires both ligand addition/removal and isomerization of the structure by ligand exchange from one site to another. Each of these transformations corresponds to multiple reaction elementary steps. We explored these elementary reactions on two examples showing that these processes correspond to large overall barriers and therefore should be kinetically slow compared to the hydrogenation reaction itself. This supports the above hypothesis that catalyst interconversion leading to deactivation is a slow phenomenon.

IR simulations were performed for unreactive catalyst structures and stable methoxy intermediates, since these long-lived species are experimentally observable and allow a direct comparison between simulated and measured IR spectra. The simulated IR spectra show good agreement with experimental measurements, reflecting the rapid consumption of reactive formate species and the slow turnover of methoxy intermediates. The consistency between the simulated reactivity trend and IR with experimental observations provides strong validation of the proposed active-site ensemble model.

Our simulations therefore present the ZrO_2 on Cu catalysts for CO_2 hydrogenation to methanol as a large ensemble of configurations presenting different number of ligands or geometries, and showing highly contrasted catalytic activities. This population of catalyst structures slowly evolves with time, increasing the weight of configurations most stable for the TOF determining methoxy intermediates, and therefore less active, providing a potential mechanism of deactivation. This statistical and dynamic view of the catalytic active sites should also apply to a wide range of highly dispersed supported catalysts, and defines an innovative direction of research for catalysis science.

Acknowledgement

This work was supported by the U.S. Department of Energy, Office of Science, Basic Energy Sciences Program under grant DE-SC0019152. Computational resources were provided by the Innovative and Novel Computational Impact on Theory and Experiment (INCITE) program at the Argonne Leadership Computing Facility, a DOE Office of Science User Facility operated under Contract DE-AC02-06CH11357. Additional calculations were carried out on the Expanse Supercomputer and Bridges2 cluster through ACCESS allocation CHE170060, supported by the National Science Foundation.

References

[1] D. S. Jenkinson, D. E. Adams, A. Wild, *Nat.* **1991**, *351*, 304-306.
[2] J. Hansen, M. Sato, R. Ruedy, K. Lo, D. W. Lea, M. Medina-Elizade, *Proc. Natl. Acad. Sci. U. S. A.* **2006**, *103*, 14288-14293.
[3] Y. Wang, L. Tan, M. Tan, P. Zhang, Y. Fang, Y. Yoneyama, G. Yang, N. Tsubaki, *ACS Catal.* **2019**, *9*, 895-901.
[4] S. Kar, R. Sen, A. Goeppert, G. K. S. Prakash, *J. Am. Chem. Soc.* **2018**, *140*, 1580-1583.
[5] S. Li, Z. Yao, F. Shang, M. Li, Y. Wei, S. Li, *Phys. Fluids.* **2025**, *37*, 013351.
[6] S. Li, F. Dang, K. Du, Z. Wang, L. Liu, S. Li, *Langmuir* **2026**.
[7] K. Lee, H. Yan, Q. Sun, Z. Zhang, N. Yan, *Acc. Mater. Res* **2023**, *4*, 746-757.
[8] G. A. Olah, *Angew. Chem. Int. Ed.* **2005**, *44*, 2636-2639.
[9] J. Graciani, K. Mudiyanselage, F. Xu, A. E. Baber, J. Evans, S. D. Senanayake, D. J. Stacchiola, P. Liu, J. Hrbek, J. F. Sanz, J. A. Rodriguez, *Science* **2014**, *345*, 546-550.

[10] C. Xie, H. Tian, H. Dai, L. Zhang, W. Long, P. Dong, Y. Wang, Y. Wang, W. Lu, N. Jin, *Appl. Therm. Eng.* **2026**, *287*, 129437.
[11] Y. Xu, Z. Gao, Y. Xu, X. Qin, X. Tang, Z. Xie, J. Zhang, C. Song, S. Yao, W. Zhou, D. Ma, L. Lin, *Appl. Catal. B Environ. Energy.* **2024**, *344*, 123656.
[12] D. Li, F. Xu, X. Tang, S. Dai, T. Pu, X. Liu, P. Tian, F. Xuan, Z. Xu, I. E. Wachs, M. Zhu, *Nat. Catal.* **2022**, *5*, 99-108.
[13] A. Álvarez, A. Bansode, A. Urakawa, A. V. Bavykina, T. A. Wezendonk, M. Makkee, J. Gascon, F. Kapteijn, *Chem. Rev.* **2017**, *117*, 9804-9838.
[14] X. Jiang, X. Nie, X. Guo, C. Song, J. G. Chen, *Chem. Rev.* **2020**, *120*, 7984-8034.
[15] J. Zhong, X. Yang, Z. Wu, B. Liang, Y. Huang, T. Zhang, *Chem. Soc. Rev.* **2020**, *49*, 1385-1413.
[16] K. Larmier, W.-C. Liao, S. Tada, E. Lam, R. Verel, A. Bansode, A. Urakawa, A. Comas-Vives, C. Copéret, *Angew. Chem. Int. Ed.* **2017**, *56*, 2318-2323.
[17] W. Wang, Z. Qu, L. Song, Q. Fu, *J. Energy Chem.* **2020**, *40*, 22-30.
[18] J. Yu, S. Liu, X. Mu, G. Yang, X. Luo, E. Lester, T. Wu, *Chem. Eng. J.* **2021**, *419*, 129656.
[19] Y. Xu, M. Wang, Z. Xie, D. Tian, G. Sheng, X. Tang, H. Li, Y. Wu, C. Song, X. Gao, S. Yao, D. Ma, L. Lin, *Chem. Eng. J.* **2023**, *470*, 144006.
[20] M. Behrens, F. Studt, I. Kasatkin, S. Kühl, M. Hävecker, F. Abild-Pedersen, S. Zander, F. Girgsdies, P. Kurr, B.-L. Kniep, M. Tovar, R. W. Fischer, J. K. Nørskov, R. Schlögl, *Science* **2012**, *336*, 893-897.
[21] S. Kuld, M. Thorhauge, H. Falsig, C. F. Elkjær, S. Helveg, I. Chorkendorff, J. Sehested, *Science* **2016**, *352*, 969-974.
[22] Y. Ma, J. Wang, K. R. Goodman, A. R. Head, X. Tong, D. J. Stacchiola, M. G. White, *J. Phys. Chem. C.* **2020**, *124*, 22158-22172.
[23] G. Wang, D. Mao, X. Guo, J. Yu, *Int. J. Hydrogen Energy* **2019**, *44*, 4197-4207.
[24] T. Pinheiro Araujo, G. Giannakakis, J. Morales-Vidal, M. Agrachev, Z. Ruiz-Bernal, P. Preikschas, T. Zou, F. Krumeich, P. O. Willi, W. J. Stark, R. N. Grass, G. Jeschke, S. Mitchell, N. Lopez, J. Perez-Ramirez, *Nat. Commun.* **2024**, *15*, 3101.
[25] X. Zhang, J.-X. Liu, B. Zijlstra, I. A. W. Filot, Z. Zhou, S. Sun, E. J. M. Hensen, *Nano Energy* **2018**, *43*, 200-209.
[26] J. A. Rodriguez, J. Graciani, J. Evans, J. B. Park, F. Yang, D. Stacchiola, S. D. Senanayake, S. Ma, M. Pérez, P. Liu, J. F. Sanz, J. Hrbek, *Angew. Chem. Int. Ed.* **2009**, *48*, 8047-8050.
[27] J. A. Rodriguez, P. Liu, J. Graciani, S. D. Senanayake, D. C. Grinter, D. Stacchiola, J. Hrbek, J. Fernández-Sanz, *J. Phys. Chem. Lett.* **2016**, *7*, 2627-2639.
[28] Y. Li, Y. Zhang, K. Qian, W. Huang, *ACS Catal.* **2022**, *12*, 1268-1287.
[29] C. Wu, L. Lin, J. Liu, J. Zhang, F. Zhang, T. Zhou, N. Rui, S. Yao, Y. Deng, F. Yang, W. Xu, J. Luo, Y. Zhao, B. Yan, X.-D. Wen, J. A. Rodriguez, D. Ma, *Nat. Commun.* **2020**, *11*, 5767.
[30] S. Kattel, B. Yan, Y. Yang, J. G. Chen, P. Liu, *J. Am. Chem. Soc.* **2016**, *138*, 12440-12450.
[31] Z. Yang, S. Kumari, A. N. Alexandrova, P. Sautet, *JACS* **2025**, *147*, 15294-15306.
[32] S. Kumari, A. N. Alexandrova, P. Sautet, *J. Am. Chem. Soc.* **2023**, *145*, 26350-26362.
[33] S. Kozuch, S. Shaik, *Acc. Chem. Res.* **2011**, *44*, 101-110.
[34] P. E. Blöchl, *Phys. Rev. B* **1994**, *50*, 17953-17979.
[35] G. Kresse, J. Furthmüller, *Phys. Rev. B* **1996**, *54*, 11169-11186.
[36] J. P. Perdew, K. Burke, M. Ernzerhof, *Phys. Rev. Lett.* **1996**, *77*, 3865-3868.
[37] S. N. Steinmann, C. Corminboeuf, *J. Chem. Phys.* **2011**, *134*, 044117.
[38] A. R. Puigdollers, F. Illas, G. Pacchioni, *J. Phys. Chem. C.* **2016**, *120*, 4392-4402.
[39] G. Henkelman, H. Jónsson, *J. Chem. Phys.* **2000**, *113*, 9978-9985.
[40] P. Poths, G. Li, T. Masubuchi, H. W. T. Morgan, Z. Zhang, A. N. Alexandrova, S. L. Anderson, *ACS Catal.* **2023**, *13*, 1533-1544.
[41] G. Sun, J. T. Fuller, III, A. N. Alexandrova, P. Sautet, *ACS Catal.* **2021**, *11*, 1877-1885.
[42] J. Yoshihara, C. T. Campbell, *J. Catal.* **1996**, *161*, 776-782.

TOC:

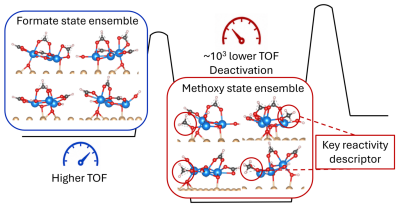

An ensemble of configurations control the activity and deactivation for CO_2 hydrogenation to methanol on inverse ZrO_2 on Cu catalysts